NASA/TM—2003-212215

A Study of Fan Stage/Casing Interaction Models

Charles Lawrence and Kelly Carney
Glenn Research Center, Cleveland, Ohio

Vicente Gallardo
Ohio Aerospace Institute, Brook Park, Ohio

March 2003

The NASA STI Program Office . . . in Profile

Since its founding, NASA has been dedicated to the advancement of aeronautics and space science. The NASA Scientific and Technical Information (STI) Program Office plays a key part in helping NASA maintain this important role.

The NASA STI Program Office is operated by Langley Research Center, the Lead Center for NASA's scientific and technical information. The NASA STI Program Office provides access to the NASA STI Database, the largest collection of aeronautical and space science STI in the world. The Program Office is also NASA's institutional mechanism for disseminating the results of its research and development activities. These results are published by NASA in the NASA STI Report Series, which includes the following report types:

- TECHNICAL PUBLICATION. Reports of completed research or a major significant phase of research that present the results of NASA programs and include extensive data or theoretical analysis. Includes compilations of significant scientific and technical data and information deemed to be of continuing reference value. NASA's counterpart of peer-reviewed formal professional papers but has less stringent limitations on manuscript length and extent of graphic presentations.

- TECHNICAL MEMORANDUM. Scientific and technical findings that are preliminary or of specialized interest, e.g., quick release reports, working papers, and bibliographies that contain minimal annotation. Does not contain extensive analysis.

- CONTRACTOR REPORT. Scientific and technical findings by NASA-sponsored contractors and grantees.

- CONFERENCE PUBLICATION. Collected papers from scientific and technical conferences, symposia, seminars, or other meetings sponsored or cosponsored by NASA.

- SPECIAL PUBLICATION. Scientific, technical, or historical information from NASA programs, projects, and missions, often concerned with subjects having substantial public interest.

- TECHNICAL TRANSLATION. English-language translations of foreign scientific and technical material pertinent to NASA's mission.

Specialized services that complement the STI Program Office's diverse offerings include creating custom thesauri, building customized databases, organizing and publishing research results . . . even providing videos.

For more information about the NASA STI Program Office, see the following:

- Access the NASA STI Program Home Page at ***http://www.sti.nasa.gov***

- E-mail your question via the Internet to help@sti.nasa.gov

- Fax your question to the NASA Access Help Desk at 301–621–0134

- Telephone the NASA Access Help Desk at 301–621–0390

- Write to:
  NASA Access Help Desk
  NASA Center for AeroSpace Information
  7121 Standard Drive
  Hanover, MD 21076

NASA/TM—2003-212215

A Study of Fan Stage/Casing Interaction Models

Charles Lawrence and Kelly Carney
Glenn Research Center, Cleveland, Ohio

Vicente Gallardo
Ohio Aerospace Institute, Brook Park, Ohio

National Aeronautics and
Space Administration

Glenn Research Center

March 2003

Available from

NASA Center for Aerospace Information
7121 Standard Drive
Hanover, MD 21076

National Technical Information Service
5285 Port Royal Road
Springfield, VA 22100

Available electronically at http://gltrs.grc.nasa.gov

A Study of Fan Stage/Casing Interaction Models

Charles Lawrence and Kelly Carney
National Aeronautics and Space Administration
Glenn Research Center
Cleveland, Ohio 44135

Vincente Gallardo
Ohio Aerospace Institute
Brook Park, Ohio 44142

Introduction

One of the primary concerns of aircraft structure designers is the accurate simulation of the blade-out event. Simulation of the blade-out event is required to pass Federal Aviation Administration (FAA) certification and to insure that the aircraft is safe for operation. Typically, the most severe blade-out occurs when a first stage fan blade in a high bypass gas turbine engine is released. Structural loading results from both the impact of the blade onto the containment ring and the subsequent instantaneous unbalance of the rotating components. Reliable simulations of the blade-out event are required to ensure structural integrity during flight as well as to guarantee successful blade-out certification testing. The loads generated by these analyses are critical to the design teams for several components of the airplane structures including engine, nacelle, strut, and wing, as well as the aircraft fuselage.

Currently, a collection of simulation tools is used for aircraft structural design (References 1,2,3). Detailed high fidelity simulation tools are used to capture the structural loads resulting from blade loss, then these loads are used as input into an overall system model that includes complete structural models of both the engines and the airframe. The detailed simulation (Figure 1) includes the time dependent trajectory of the lost blade and it's interactions with the containment structure while the system simulation

includes the lost blade loadings and the interactions between the rotating turbomachinery and the remaining aircraft structural components. General-purpose finite element structural analysis codes are typically used and special provisions are made to include transient effects from the blade loss and rotational effects resulting from the engine's turbomachinery.

An area of particular importance to the simulation process is capturing the interactions between the fan blades and the casing. Typically, the system simulation will employ some form of interaction model to characterize the fan blade to case interactions during impact and post impact rub that occurs as a result of the rotor being out of balance. High fidelity simulation tools (e.g. LS-DYNA) have the potential to capture the details of fan blade-case interactions including effects such as rub, damage, wear and friction, however, the interaction must be characterized in a simpler manner that is compatible with the large scale system simulation. While the detailed simulation may predict the three-dimensional nonlinear behavior of the blades contacting the case, the system model needs to simulate the gross macro behavior using a simpler model that consists of a flexible rotor modeled with beam elements and lumped concentrated masses for the bladed disk, since this is the type of modeling that is normally used for the system simulation. The purpose of the present study is to investigate the performance of several existing and new, blade-case interactions modeling capabilities that are compatible with the large system modeling strategy but are able to capture the complex blade-case interactions with enough fidelity for an accurate system simulation.

Comparison of NASTRAN Nonlinear Radial Gap Element and CGAP Elements

The first two interaction models that are studied in the present study are the Nonlinear Radial Gap (NLRGAP) and the CGAP Elements currently available in NASTRAN (References 4, 5). The CGAP is a one dimensional element used to model a gap and associated friction between two nodes while the NLRGAP element is used to model a gap and friction in a plane such as might occur with a shaft moving inside a bearing support. These two models are commonly used by the industry to simulate blade-case interactions. In practice both of these element types may be used to model

the interactions between the rotor and stationary components (e.g. bearing housing or shroud) resulting from steady state or sudden unbalance. The NLRGAP provides a convenient modeling tool for these problems in that only a single element is needed to model the interactions. The major limitation of the NLRGAP is that since only a single NLRGAP is used the rotor must be connected to only a single point on the supporting structure. For structural supports having symmetry this limitation may not present a problem but for non-symmetric bearing supports or rotor shrouds simplifying approximations must be made. Unlike the single NLRGAP, the use of the CGAP element to model rotor interactions requires that a number of CGAP elements be placed around the circumference of the rotor. Since this element is one dimensional, a number of them must be distributed around the circumference of the rotor to support rotor motion in all the radial directions. There are three parameters associated with the CGAP and NLRGAP elements; gap clearance, gap radial stiffness, and gap friction coefficient. The radial stiffness produces a radial force once the gap clearance is closed while the friction force produces a tangential force that is proportional to the radial force and in the direction opposite to the rotation of the rotor. In general, the NLRGAP element is simpler to implement than the CGAP and is effective for modeling contact, however, as mentioned previously it can only be connected to a single point on the case so the NLRGAP element cannot accommodate flexible cases where the shape of the case does not remain round.

A simple cantilevered rotor was used to compare the NLRGAP to the CGAP element. Figure 2 shows the finite element model. The model consists of 5 beam elements, 6 nodes and 36 degrees of freedom. Relatively rigid springs attach node 6 to ground in both the translational and rotational directions. Although axial and torsional degrees of freedom are included in the finite element model they are not used in the present study. All of the rotational inertias (I_p, I_α, I_θ) are concentrated in the disk at the rotor attachment point. The present model is identical to the model used by Boeing in "Sample Problem One" of their documentation for rotordynamic analysis (Reference 6).

Transient simulations of a blade loss event were performed to compare the NLRGAP to the CGAP elements. A blade loss event is simulated by applying a mass unbalance at the rotor tip at time = 0.0 seconds. Initially, the rotor is

spinning at full speed. Just beyond 0.0 seconds, after the blade loss, the rotor begins to slow until it reaches zero speed at 1.0 seconds. Since the centrifugal force from the unbalance is a function of rotor speed it also diminishes to zero at 1.0 seconds. Gyroscopic effects are included in the simulation.

Figures 3a and 3b show results from the simulations. Displacement curves are shown for the NLRGAP and for three different CGAP configurations consisting of 4, 8 and 32 CGAP elements. The sum of the stiffnesses of the CGAP elements was made to equal the stiffness of the single NLRGAP for a zero gap condition in an attempt to match the results from the CGAP models to those of the NLRGAP. The gap in both the NLRGAP and CGAP was set to 0.4 inches and no friction forces were implemented.

The results show that for up to approximately 0.08 seconds the results for all of the models are identical. This is expected since the magnitude of the displacement is less than the gap opening of 0.4 inches and the NLRGAP and CGAP's are having no effect. Beyond 0.08 seconds the rotor displacement exceeds the gap opening and the NLRGAP and CGAP's begin to exert a radial restoring force on the rotor. At this point, the results from the NLRGAP model show an additional displacement of approximately 0.05 inches before the displacements decay downward to near zero at 1.0 seconds.

The trajectory of the rotor tip for the CGAP models with 8 and 32 CGAP elements follow the same path as the trajectory for the NLRGAP model except that the magnitude of the trajectory is slightly larger for the CGAP models. It was expected that as the number of CGAP's increased the solution obtained with the CGAP's would converge to the solution obtained with the NLRGAP. However, after further consideration it was realized that the two approaches will never be exactly identical since the NLRGAP gap opening is always in the direction of the rotor motion while the gap in the CGAP's may or may not be parallel to the direction of the rotor motion. As a result of this geometric nonlinear effect, for a given rotor displacement the gap in the NLRGAP may be closed while the gap in some of the CGAP may still be open, or not closed as much, and therefore not applying the same force as the NLRGAP.

The results for the model with only four CGAP elements do not match the results of the other models. With only four CGAP elements, the proper rotor tip trajectory is not computed since the distribution of the elements does not provide a fine enough distribution of the gap or restoring forces. As a result, while some rotor lateral displacements are oriented in the direction of a gap element and are resisted by the gap restoring force other displacements are "between" elements and do not experience any, or experience less, effect from the gap elements. Because of this off and on effect from using too few gap elements there also is an impacting effect that causes the rotor displacements to oscillate more than if the gap elements were more evenly distributed around the circumference of the rotor.

The next step in the present study was to examine the effects of element parameters (e.g. radial stiffness, friction coefficient and gap distance) on the rotordynamic response. To perform this part of the study a stand-alone rotordynamic FORTRAN code was developed. A separate rotordynamic code was developed because some features associated with fan stage-case interactions models are not readily available in commercial codes such as NASTRAN. The code was validated by comparing a Campbell diagram generated from the FORTRAN code to results obtained from NASTRAN. Figure 4 shows the Campbell diagram comparison for the first forward and backward mode of the sample rotor. The 1/rev line shown in this figure indicates the first critical speed at 3000 RPM. As shown in the figure, there is perfect agreement between the NASTRAN and FORTRAN program generated results thus verifying that the rotordynamic code is correctly predicting the rotordynamic response, at least where there is no interaction between the fan stage and case.

A gap element, which is identical to the CGAP element currently available in NASTRAN, was incorporated into the code to assess the effects of the gap parameters and rotor speed. Figure 5 shows orbit plots at the rotor tip for four rotor rotational speeds (2000, 4000, 6000, and 8000 RPM). For these results the gap clearance was made large so there is no contact between the rotor and case and therefore no radial contact or tangential friction forces. The orbits are minimum at 2000 RPM, increase at 4000 RPM then decrease up to 8000 RPM. Even though the unbalance load is greatest at 8000 RPM, this decreased response is expected since the rotor first critical speed

which is at 3000 RPM is close to 4000 RPM, and no critical speed near 8000 RPM exists.

Figure 6 shows orbit plots where the gap clearance and radial stiffness was set to 0.20 inches and 5.0 x 10^5 lb./inch, respectively. The friction coefficient remained at 0.0 so although there is a radial gap force present when the gap clearance is exceeded a tangential friction force is never produced. As expected the orbits in this figure are smaller and more contained than the orbits in the previous figure since there is a restoring force whenever the rotor displacements exceed the gap of 0.20 inches. The resonant condition that was evident in the previous figure does not appear in this figure since the restoring force disrupts the resonant behavior. Unlike the previous figure where the largest orbits matched the critical speed, the maximum orbits for these results coincide with the maximum unbalance force at 8000 RPM.

Figures 7 and 8 show transient and orbit plots where the gap clearance and radial stiffness was set to the same values as in the previous figure but the friction coefficient was 0.10 thus introducing a tangential friction force. Similarly to the previous simulations where the friction coefficient was set to 0.0 and there was no friction force, the rotor displacements are constrained by the casing. However, for this case the orbits are much more chaotic as a result of the friction force. The friction force, which is proportional to the rotor displacement but 90 degrees out of phase with the displacement appears similar to internal rotor damping and causes chaotic motion in more extreme cases. When the rotor speed is higher or the friction force is greater the rotor motions will become unstable. In practice this phenomenon may be somewhat tempered since for real rotors as the rotor motion becomes large the radial stiffness and overall damping may actually increase and/or the rotor may become damaged so it can no longer sustain as large a tangential destabilizing force. This phenomenon poses a limitation for the currently used interaction elements, such as the CGAP or NLRGAP, since they do not account for these nonlinear effects.

Rigid Bladed Disk Model with Friction Rub

The model used for the previously discussed results utilized a rigid disk without blades. The next step in the present study is to implement discrete rigid blades into the rigid disk. For this model the contact between the bladed disk and case is intermittent occurring only where blades are located and the gap is closed, whereas in the previous model the contact is continuous as long as the gap is closed. Figure 9 depicts the methodology used for the rigid bladed disk. The penetration distance, $\vec{r}_p$ is calculated using the displacement of the center of the disk, the angular position of the blade of interest and the radius of the case.

The distance from the origin to the blade tip is:

$$\left|\vec{r}_c + \vec{r}_p\right| = \left|\vec{r}_u + \vec{r}_b\right| \tag{1}$$

Where $\vec{r}_c$ is the radius of the case, $\vec{r}_p$ is the penetration of the blade into the case, $\vec{r}_u$ is the displacement of the bladed disk at the rotor attachment point (obtained directly from the rotor degrees of freedom) and $\vec{r}_b$ is the radius of the blade tip. For the present study the case is assumed to be rigid and fixed to ground so $\vec{r}_c$ is a constant

Since $\vec{r}_p$ and $\vec{r}_c$ are collinear, the penetration distance may be obtained by rearranging equation (1) as:

$$\left|\vec{r}_p\right| = \left|\vec{r}_c + \vec{r}_p\right| - \left|\vec{r}_c\right| \tag{2}$$

The distance $\left|\vec{r}_c + \vec{r}_p\right|$ can be determined by:

$$\left|\vec{r}_c + \vec{r}_p\right| = \sqrt{(\left|\vec{r}_b\right|\cos\beta + u_x)^2 + (\left|\vec{r}_b\right|\sin\beta + u_y)^2} \tag{3}$$

Where β is the angle to the blade (assuming synchronous vibration, $\beta = \psi$), and u_x and u_y are the horizontal and vertical displacements of the rotor at the disk attachment point (Figure 9).

Substituting equation 3 into 2 yields:

$$\left|\vec{r}_p\right| = \sqrt{(\left|\vec{r}_b\right|\cos\beta + u_x)^2 + (\left|\vec{r}_b\right|\sin\beta + u_y)^2} - \left|\vec{r}_c\right| \tag{4}$$

At each point in time every blade on the disk is checked to see if the blade has penetrated the case. If penetration exists, then a radial force that is parallel to the vector, $\vec{r}_c$ and a tangential force which is perpendicular to $\vec{r}_c$, is calculated.

Figure 10 shows results for the rigid disk with 16 rigid blades. Figure 10a can be compared to Figure 6c and Figure 10b can be compared to Figure 8c. These comparisons are relevant because the simulations were generated with the same loadings and rub characteristics, the only difference being the results in Figures 6 and 8 used the rigid disk without blades while the results in Figure 10 were generated using a disk with rigid blades. The comparison of these results shows that there is negligible difference between using a model with a rigid disk versus a model with a rigid disk with rigid blades. A likely explanation for the similarity is that the bladed disk has a large enough number of blades such that the spacing between blades is small and the bladed disk behaves as a continuous disk. Although not shown, a similar simulation with only four blades on the disk did exhibit very different results from the results for the disk without blades.

Individual Blade Plowing Model

Limited data and experience with rub tests on turbofan engines and test rigs indicate that blade tip rub forces, resulting from blade tip and case interactions, are in a direction that is perpendicular to the blade tip chordline. This phenomenon is similar to the behavior of an airfoil traveling through a fluid where the airfoil motion generates a lift and drag forces. From tests, the tangential rub blade force was found to have an axial component that would move the blade forward (or aft), and a circumferential component that opposes the rotor rotation. The hydrodynamic analogy expresses the blade rub force as proportional to the blade tip's mean velocity and the instantaneous angle of attack or incidence. It differs from the typically used friction model of rub in that the friction model only generates a force in the direction opposing the rotor spin (i.e.

drag) while the plowing model generates this drag force, as well as a "lifting" force that is perpendicular to the direction of rotor spin.

An analytical expression, analogous to the dynamic pressure force from a change in momentum is used to develop the plowing model. This model is consistent with expressions of impact forces and hydrodynamic pressure. (Reference 7) This was necessitated by the observed directionality of the blade tip "tangential" rub forces, i.e., perpendicular to the blade chordline.

The hydrodynamic force is defined as:

$$f = DV^2\gamma_t A \tag{5}$$

where f is the total tangential force on the blade from rubbing, V is the blade tip velocity, γ_t is the blade chordline angle of incidence in the rotating frame, and A is the frontal area of the rubbing material (i.e. chord length * rub depth). D is a coefficient that must be determined from test or some other analysis procedure. It is most likely a function of several factors such as the material's Young and Shear moduli, density, hardness, machinability, feed depth, dynamic shear strength, smoothness and probably others.

For the present study, a beam rotor with rigid blades and disk will be utilized. The rigid bladed disk is just a localized extension of the rotor, and has no separate degrees of freedom. Thus the vibration of the bladed disk is only the motion imparted by its attachment point on the rotor.

The incidence angle for a rigid bladed disk in the orbiting disk frame is (Reference 8):

$$\gamma_t = \gamma_0 + \alpha\sin\beta + \theta\cos\beta - \dot{w}/\psi R \tag{6}$$

Where γ_0 is the blade tip chordline mean (i.e. initial) incidence angle, α and θ are yaw and pitch displacements, β is the azimuth position of the blade from the fixed horizontal axis (Figure 9). ψ is the rotor spin speed, R is the blade tip radius, and w and $\dot{w}$ are the blade tip axial position and velocity, respectively and are defined as:

$$w = -\alpha R\cos\beta + \theta R\sin\beta \tag{7}$$

So that:

$$\dot{w} = -\dot{\alpha}R\cos\beta + \dot{\theta}R\sin\beta\ \dot{\beta}R(\alpha\sin\beta + \theta\cos\beta) \tag{8}$$

Substituting (8) into (6) the blade tip chordline angle of incidence is:

$$\gamma_t = \gamma_0 - \frac{\dot{\alpha}\cos\beta - \dot{\theta}\sin\beta}{\dot{\psi}} + (\alpha\sin\beta + \theta\cos\beta)(1 - \frac{\dot{\beta}}{\dot{\psi}}) \tag{9}$$

For synchronous vibration, $\dot{\beta} = \dot{\psi}$ and equation (9) reduces to:

$$\gamma_t = \gamma_0 - \frac{\dot{\alpha}\cos\beta - \dot{\theta}\sin\beta}{\dot{\psi}} \tag{10}$$

Substituting the total incidence angle, equation (10) into (5) yields the tangential plowing force in the orbiting reference frame:

$$f = D\dot{\psi}^2R^2(\gamma_0 - \frac{\dot{\alpha}\cos\beta - \dot{\theta}\sin\beta}{\dot{\psi}})A \tag{11}$$

Assuming that the vibratory components of the incidence angle are negligibly small, compared to the mean incidence, the axial and circumferential components of the force on the blade in the orbiting frame are:

$$f_a = f\cos\gamma_0 \qquad \text{(axial)} \tag{12}$$

$$f_t = f\sin\gamma_0 \qquad \text{(circumferential)} \tag{13}$$

The forces and moments in the rotor degrees of freedom in an inertial frame of reference can be obtained by resolving the plowing force, equation (11), into the three orthogonal components corresponding to the rotor translational degrees of freedom.

Axially,

$$f_a = f\cos\gamma_0 \quad \text{(axial)} \tag{12}$$

Horizontally,

$$f_x = f_t \sin\beta \tag{14}$$

Vertically,

$$f_y = -f_t \cos\beta \tag{15}$$

The horizontal and vertical forces yield shear forces in the direction of the rotor translational degrees of freedom, whereas the axial force produces moments about the yaw and pitch axes. The moments about the yaw and pitch axis, respectively are:

$$f_\alpha = -f_a R\cos\beta \tag{16}$$

$$f_\theta = f_a R\sin\beta \tag{17}$$

Individual Blade Radial Forces

In addition to the previously described plowing force, there is a radial force on the blades and an equal and opposite force on the case resulting from radial motion of the rotor blades. When the radial motion of the blades exceeds the gap distance, the blade tips push against the case and a restoring force is exerted back against the blades. This restoring force tends to re-center the bladed disk and its magnitude is proportional to the casing stiffness. The radial force is defined as:

$$\mathbf{f}_r = -k\vec{r}_p \tag{18}$$

Where k is the case stiffness and $\vec{r}_p$ is the penetration depth at the point of blade contact with the case. In practice $\vec{r}_p$ may vary not only from the rotor displacement, but also from the rub material getting worn away from blade contact, but in the present study only rotor displacement will be considered and blade and case displacements will not be considered.

The horizontal and vertical components of the radial force are:

$$f_{r_y} = -k\vec{r}_{p_y} \tag{19a}$$

$$f_{r_z} = -k\vec{r}_{p_z} \tag{19b}$$

Where $\vec{r}_{p_y}$ and $\vec{r}_{p_z}$ are the horizontal and vertical components of the penetration of the blade tip into the case.

Summing of Forces and Moment on all Rubbing Rigid Blades

Once the plowing and radial force is computed for each blade, the total force and moment acting on the rotor degrees of freedom are obtained by summing the forces for each of the individual blades. Each blade will contribute a different force and moment since the penetration depth and incidence angle is different for each blade.

Results for Rigid Bladed Disk Using Plowing Model

The results in Figure 11 are for an overhung rotor with a disk at the free end. The disk has 16 blades and an initial clearance of 0.2 inches between the blade tips and case. The blade tip radius is 10.0 inches. A radial restoring spring is used to model the radial behavior while the plowing model is used for the tangential loads.

For the initial results, the plowing force was kept simple by setting the blade angle of attack to a constant 90 degrees (the change in angle resulting from any vibrations was not included). The 90 degrees is not realistic, however, it eliminates any loads in the axial direction and overturning

moments so a comparison could be made to the friction model that was previously discussed in this report. The only difference between this simulation and the friction model is that in the previous model the tangential friction force is proportional to the penetration depth while in the present model the plowing force is proportional to the penetration depth and the blade tip velocity. Both the friction and plowing forces are in the same direction and oppose rotor rotation.

As shown in the figure, the simulation was run at three different speeds; 3000, 6000, and 9000 RPM. Regardless of the rotor speed, the shapes of the curves are very similar. The difference between the curves is that the displacements are larger for faster rotor speeds which are expected since the plowing force is proportional to rotor speed squared. (The loading is an unbalance that also increases with rotor speed squared). For small Dynamic Coefficients the orbital displacement is small since a small Dynamic Coefficient generates a small plowing force. As expected, as the Dynamic Coefficient increases the orbital displacement increases. For very large Dynamic Coefficients the rotor response/displacements grow very large but do not go unstable because of the 5% level of structural damping provided in the model. If the level of structural damping was decreased, or eliminated, an unstable response is obtained. Obviously, the results in this figure are not realizable since the displacements are orders of magnitude larger than the structural dimensions; however, the results do demonstrate the effect of the dynamic coefficient for extreme cases.

Figures 12 and 13 show the effect of the Dynamic Coefficient and structural damping on the displacement response. The only difference between the models used for these two figures is that the results in Figure 12 were generated using 3% structural damping while the results in Figure 13 used 1% structural damping. As previously discussed, the Dynamic Coefficient determines the magnitude of the destabilizing skew symmetric plowing force. Conversely, the structural damping provides a stabilizing force that helps to reduce the displacement response.

For smaller Dynamic Coefficients the displacement response is relatively small and levels off to a steady state in a short amount of time. (Figure 12a, 12b, Figure 13a) The steady state displacement exceeds the gap clearance because the centrifugal force is large in comparison to the stiffness of the

radial restoring spring. For this level of plowing force structural damping has minimal effect on the magnitude of the displacements.

For larger Dynamic Coefficients the plowing force is more forcibly driving the response unstable. The only reason the response does not grow exponentially is because of the structural damping. Without any structural damping the response does in fact grow exponentially, however with just 1% damping the response, although possibly quite large, is still stable. With 3% structural damping the magnitude of the response is less than with 1% damping, however the onset of large displacements is greatly influenced by the level of damping. While the onset of large displacements occurs with a Dynamic Coefficient of 5.0E-5 lbm/in**3 and 1% damping (Figure 13b), it does not occur until the Dynamic Coefficient is 1.0E-4 lbm/in**3 when the damping is 3%. (Figure 12c)

Figure 14 shows the effect of a 30 degree blade angle of attack for various values of Dynamic Coefficient. For this angle of attack, unlike an angle of attack of 90 degrees, there is a component of plowing force in both the axial, as well as the circumferential direction. The axial component produces an oscillating moment about the rotor y and z axis (Figure 9). The results in Figure 14 follow the same trend as Figure 12 where all the parameters are the same except for the angle of attack. The onset of the larger displacement is delayed for the smaller angle of attack which is expected since the magnitude of the plowing force is smaller when the angle is 30 degrees than when the angle is 90 degrees.

Figure 15 shows the gyroscopic and plowing force moments and the resulting transient response for a Dynamic coefficient of 1.e-4 lbm/in**3 and a rotor speed of 9000 RPM. For this combination of rotor speed and Dynamic Coefficient the plowing force moment is considerably smaller than the gyroscopic moment. For slower rotor speeds and large Dynamic Coefficients the moments will be closer in magnitudes. Regardless of the magnitude of these moments, the plowing force moment is always 180 degrees out of phase with the gyroscopic moment and therefore has an offsetting effect. The rotations shown in Figure 15b depict this effect by showing how the rotations are smaller when the plowing force moment is included in the simulation.

A major challenge for all of the simulations presented in this work is that although the numerical simulation is able to produce a reliable transient response for a given set of input parameters, the fidelity of the response is only as good as the quality of the input parameters (e.g. Dynamic Coefficient, structural damping). Unfortunately, these parameters are very difficult to predict in practice and as shown in the present results a small variation in the parameters may lead to large variations in the resulting response.

Summary

Three contact models have been examined for simulating the interactions between a rotor bladed disk and a case: a radial and linear gap element and a new element based on a hydrodynamic formulation. All three models were assessed using results from unbalance loadings and transient simulations. The first two models are currently available in commercial finite element codes such as NASTRAN and have been showed to perform adequately for simulating rotor-case interactions. The hydrodynamic model, although not readily available in commercial codes, may prove to be better able to characterize rotor-case interactions. Future work includes adding flexibility to the rotor case and incorporating vibratory motions into the coordinates used to define the rotor blade position, as well as experimental testing to determine which of the models are best suited for simulating rotor-case interactions.

References

1. Lawrence, C., Carney, K., Gallardo, V., "Simulation of Aircraft Engine Blade-Out Structural Dynamics," NASA/TM—2001-210957/REV1, September 2001.

2. Vasco, T.J. (2000). "Fan Blade Bird Strike Analysis and Design," 6th International LS-DYNA Users Conference.

3. Carney, K.S., Lawrence, C., Carney, D.V., "Aircraft Engine Blade-Out Dynamics," 8th International LS-DYNA Users Conference.

4. Sitton, G., "MSC/NASTRAN Basic Dynamic Analysis," The MacNeal-Schwendler Corporation, 1997.

5. Herting, D.N., "MSC/NASTRAN Advanced Dynamic Analysis User's Guide," The MacNeal-Schwendler Corporation, 1997.

6. Heidari, M.A., Carlson, D.L., Yantis, T.F. (2000), "Documentation for the Boeing Rotor Dynamics Analysis Procedure," Boeing D6-36663.

7. Streeter, V.L., Wylie, E.B., "Fluid Mechanics," McGraw-Hill, 1975.

8. Bisplinghoff, R.L., Ashley, H., "Principles of Aeroelasticity," Dover Publications, Inc., 1962.

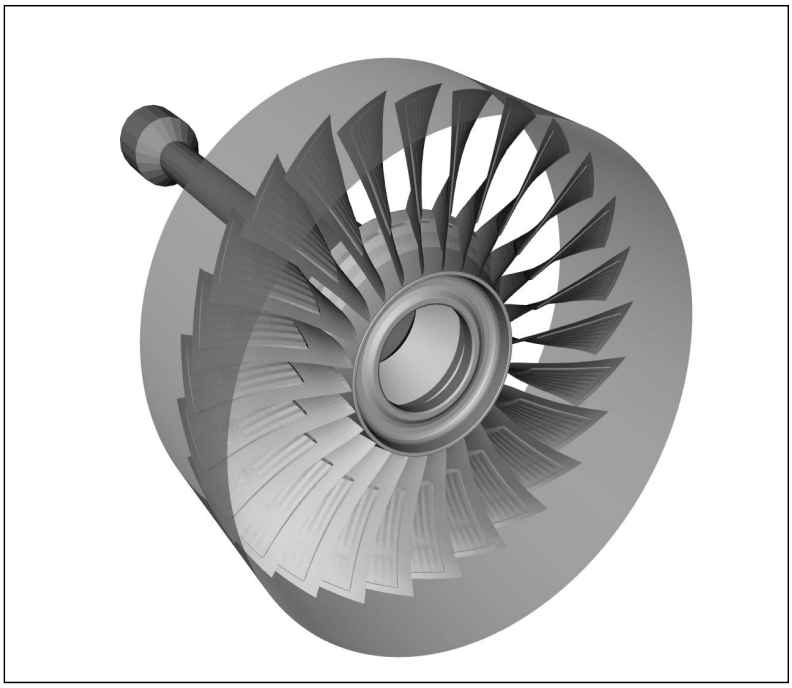

Figure 1: Detailed blade-fan case interaction model.

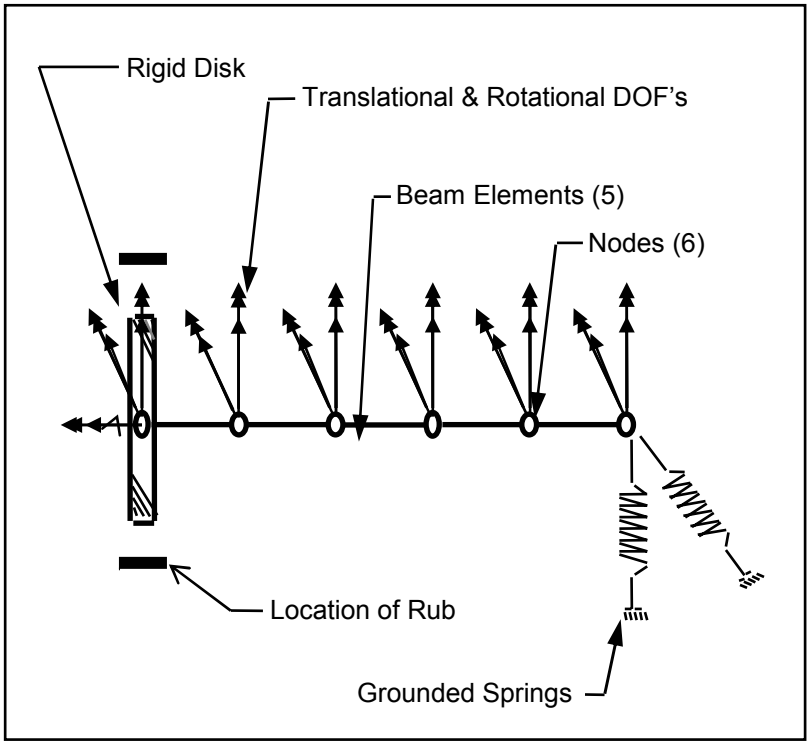

Figure 2: Rotor finite element model.

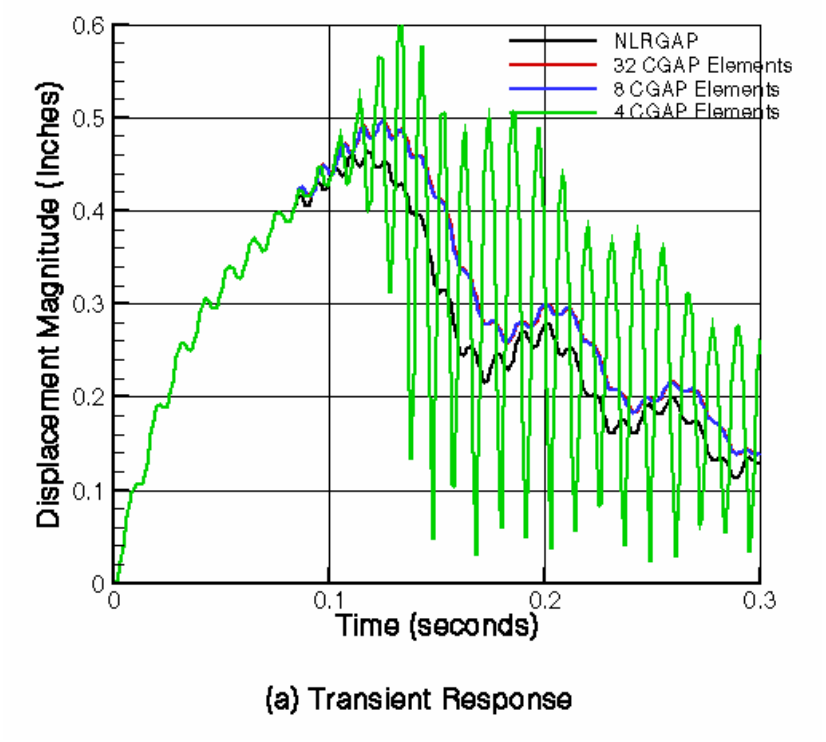

(a) Transient Response

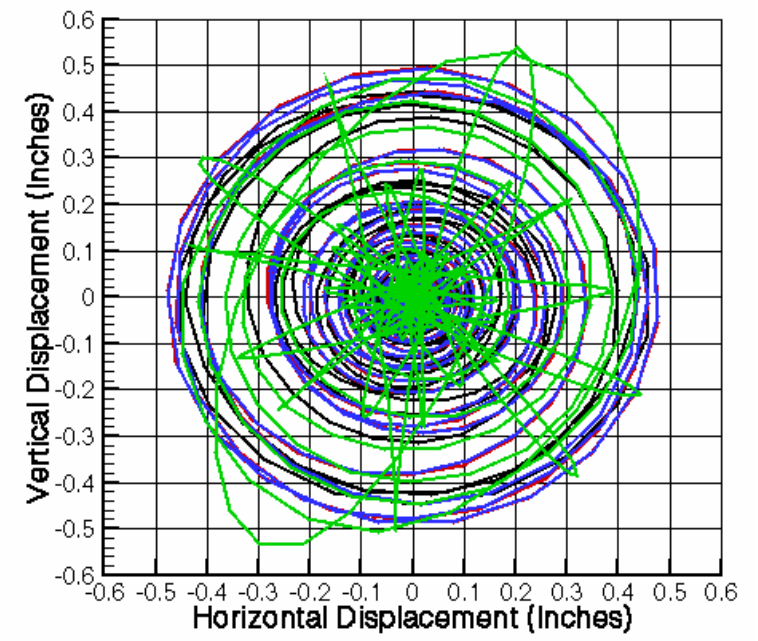

(b) Orbit Plot

Figure 3: Comparison between nonlinear radial gap (NLRGAP) and CGAP elements

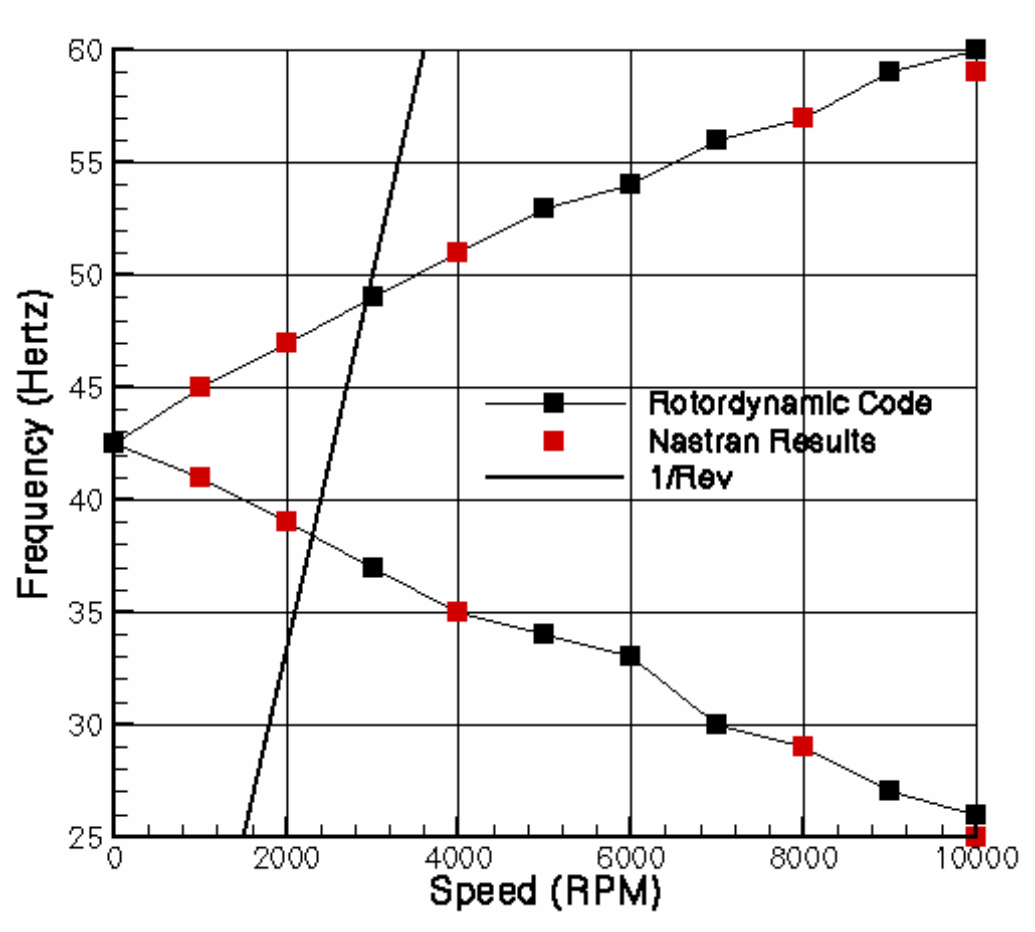

Figure 4: Rotor Campbell diagram.

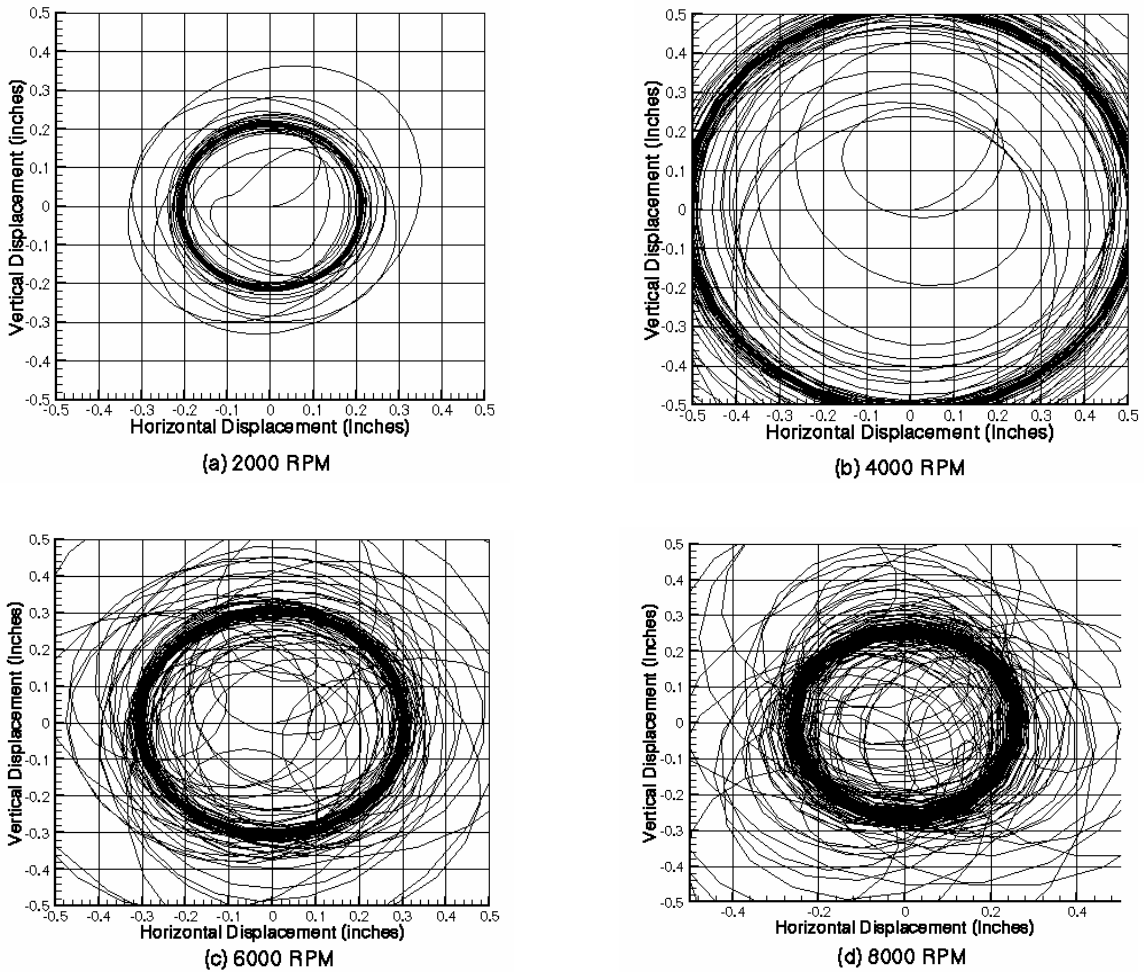

Figure 5: Rotor tip orbits for increasing rotor speed (open gap).

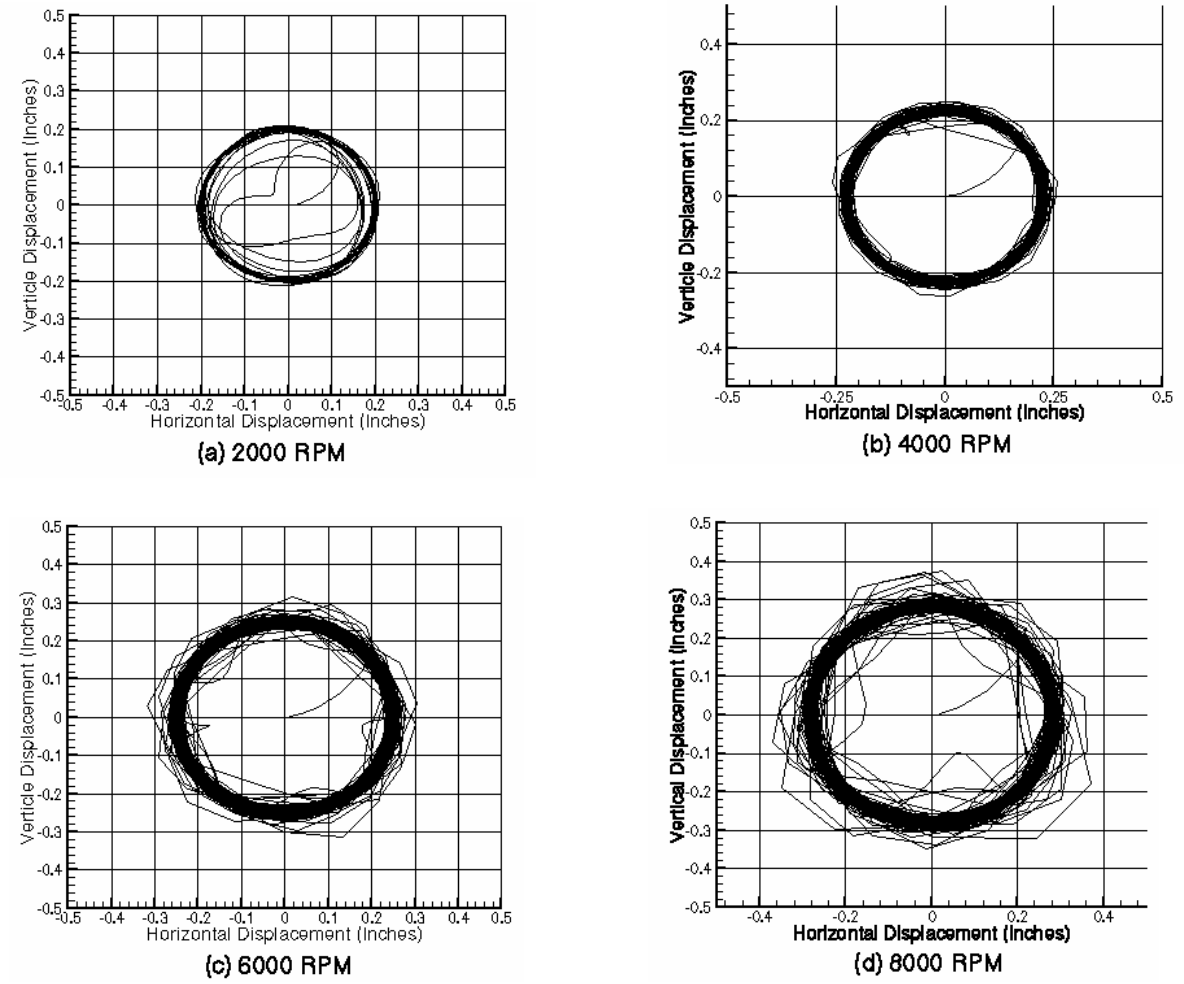

Figure 6: Rotor tip orbits for increasing rotor speed.
Gap = 0.20 inches, Stiffness = 5e05 psi, Friction coefficient = 0.0

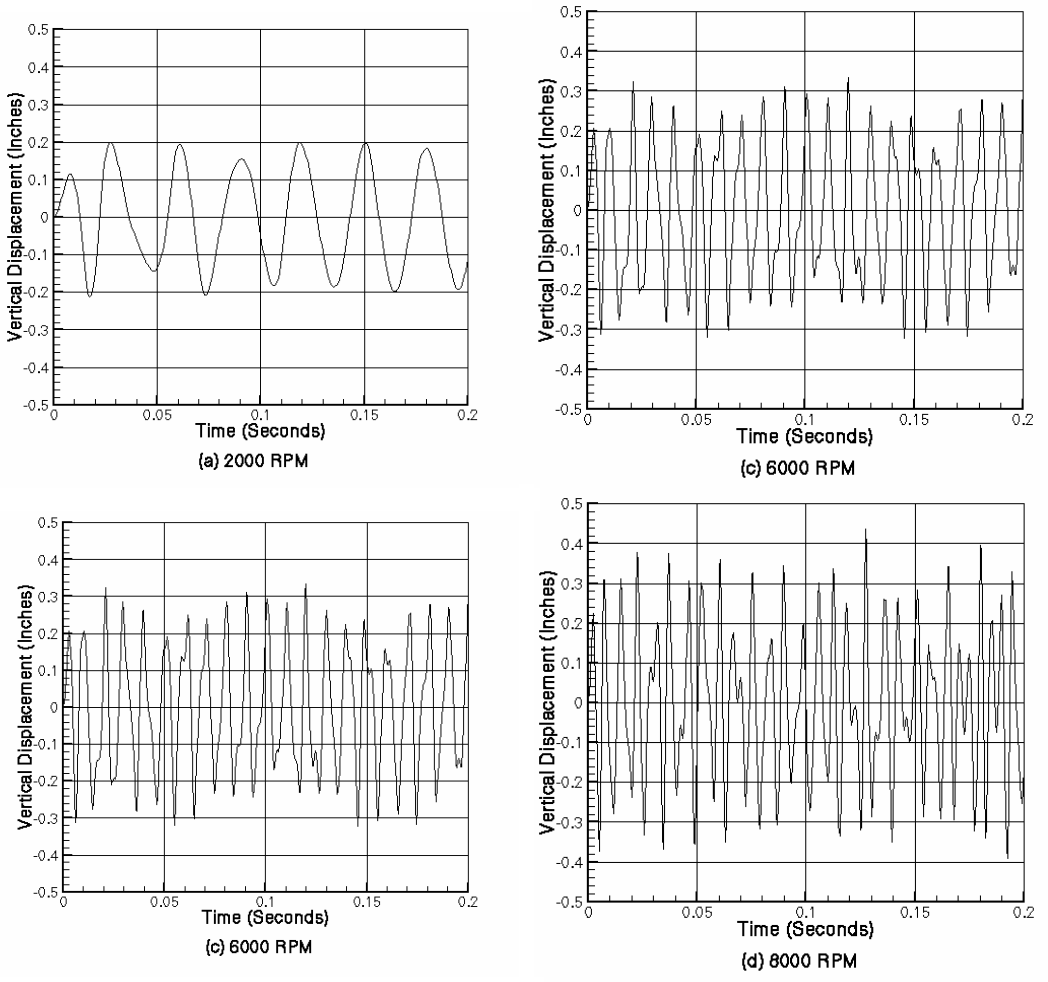

Figure 7: Rotor tip displacement for increasing rotor speed. Radial stiffness = 5.E05, Friction = 0.10, Gap = 0.20.

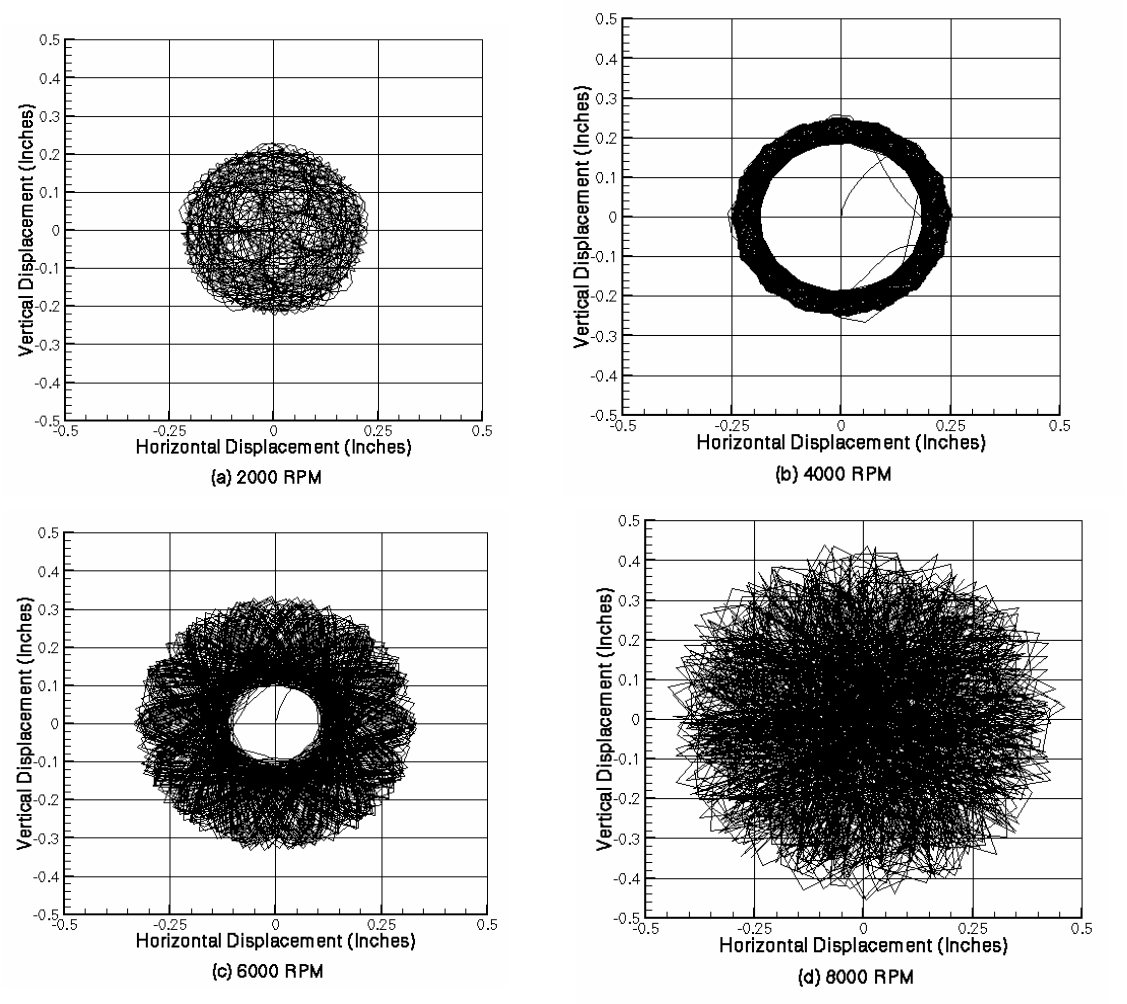

Figure 8: Rotor tip orbits for increasing rotor speed.
Radial stiffness = 5.E05, Friction = 0.10, Gap = 0.20.

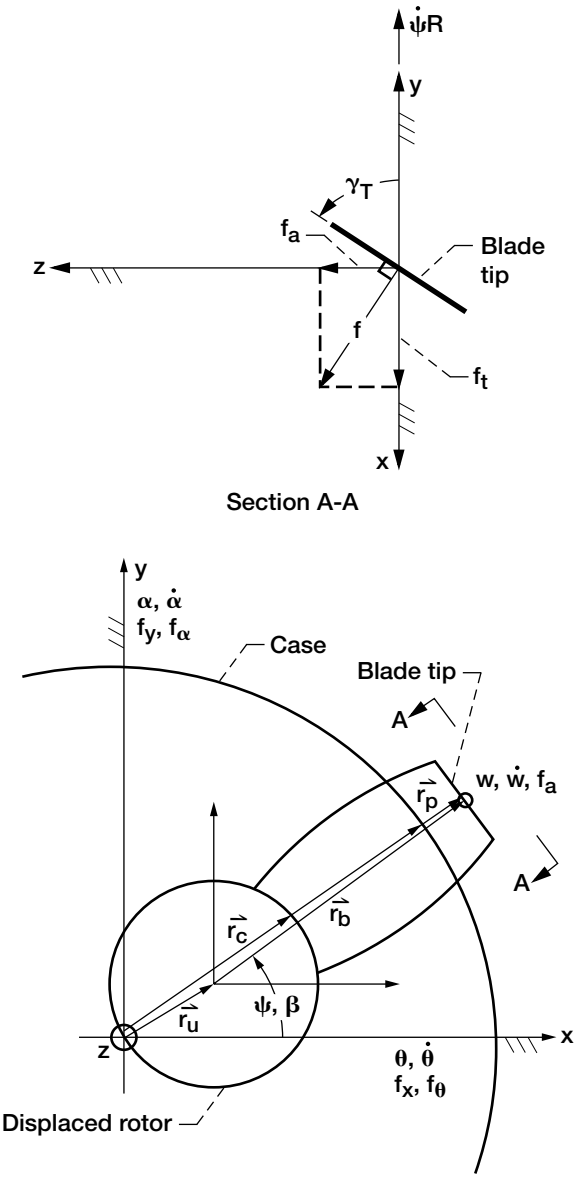

Figure 9: Schematic of rotor blade, degrees of freedom, and tip penetration.

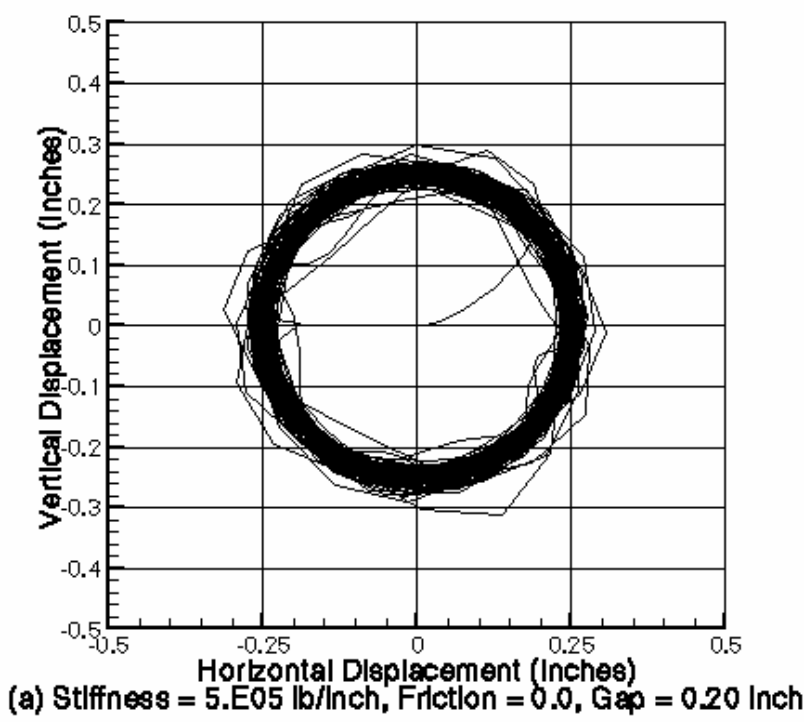

(a) Stiffness = 5.E05 lb/inch, Friction = 0.0, Gap = 0.20 inch

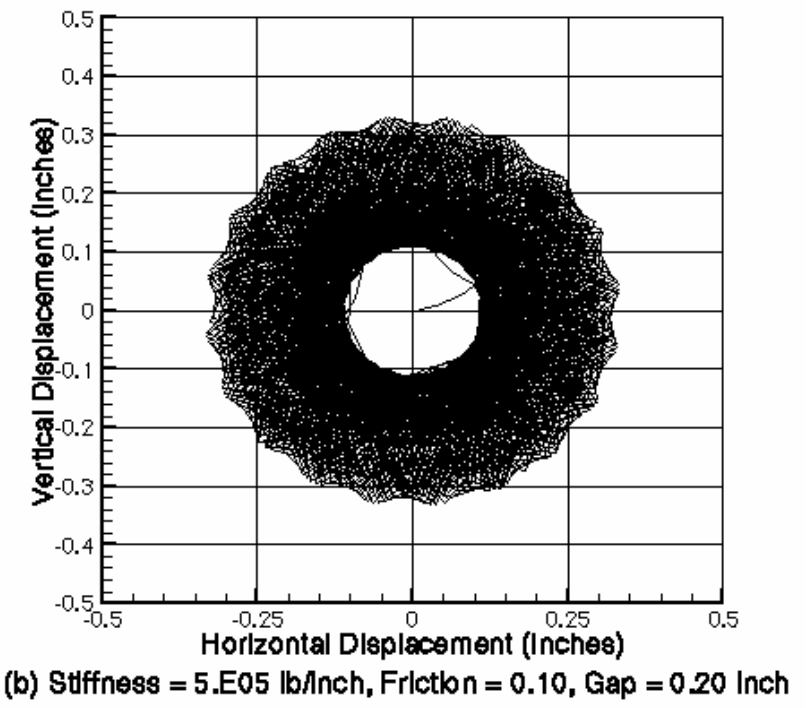

(b) Stiffness = 5.E05 lb/inch, Friction = 0.10, Gap = 0.20 inch

Figure 10: Bladed disk model with 16 blades. Rotor speed = 6000 RPM.

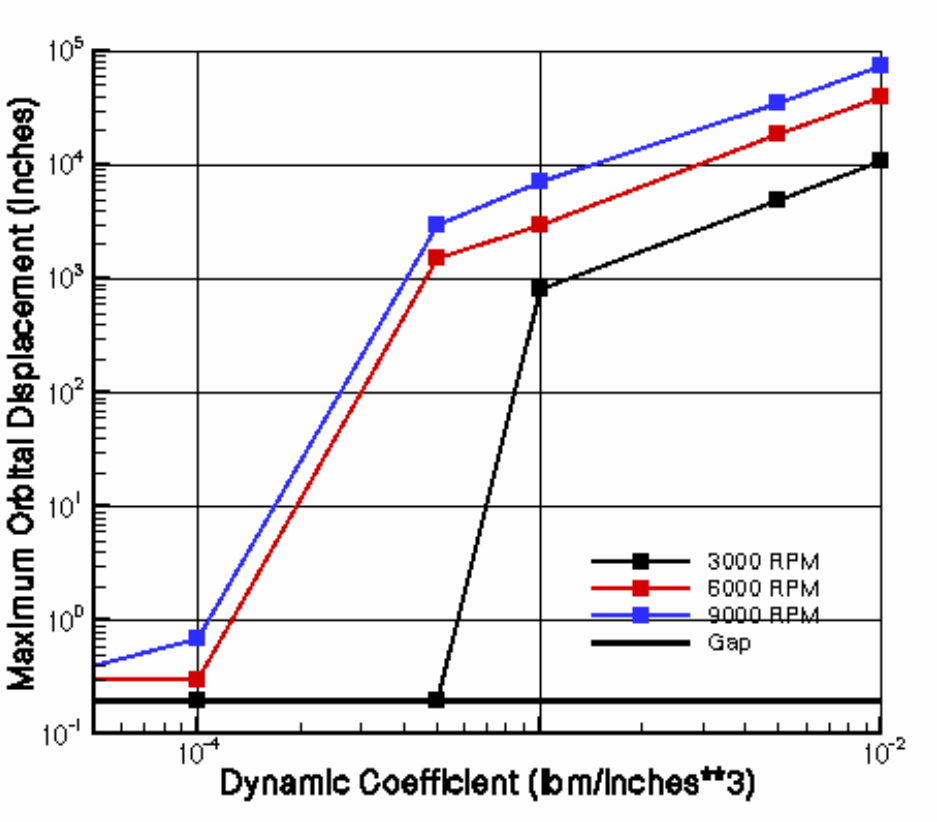

Figure 11: Maximum displacement versus dynamic coefficient. Blade angle of attack = 90 degrees, 5% damping.

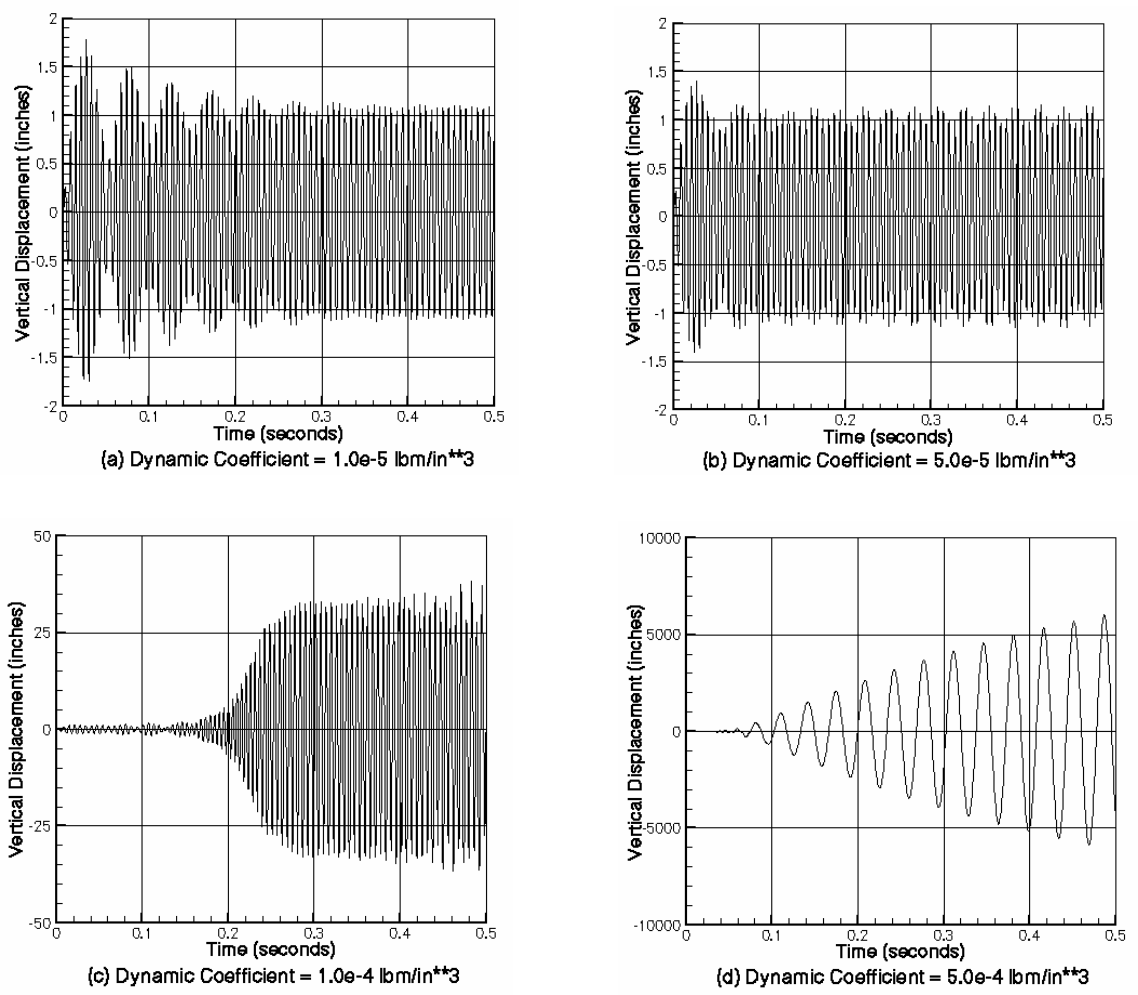

Figure 12: Effect of dynamic coefficient on transient response (3% structural damping, 90 degree angle of attack).

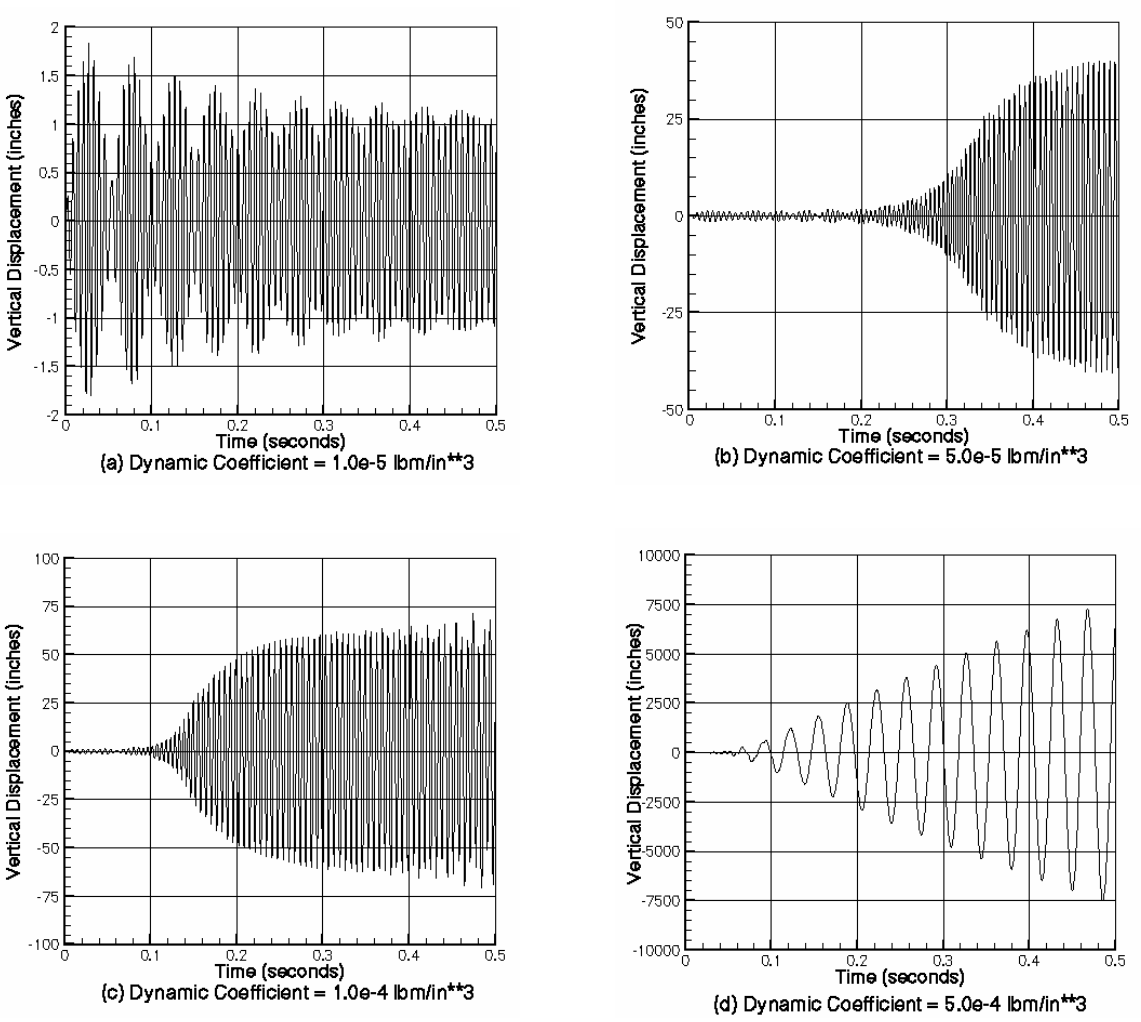

Figure 13: Effect of dynamic coefficient on transient response (3% structural damping, 30 degree blade angle of attack).

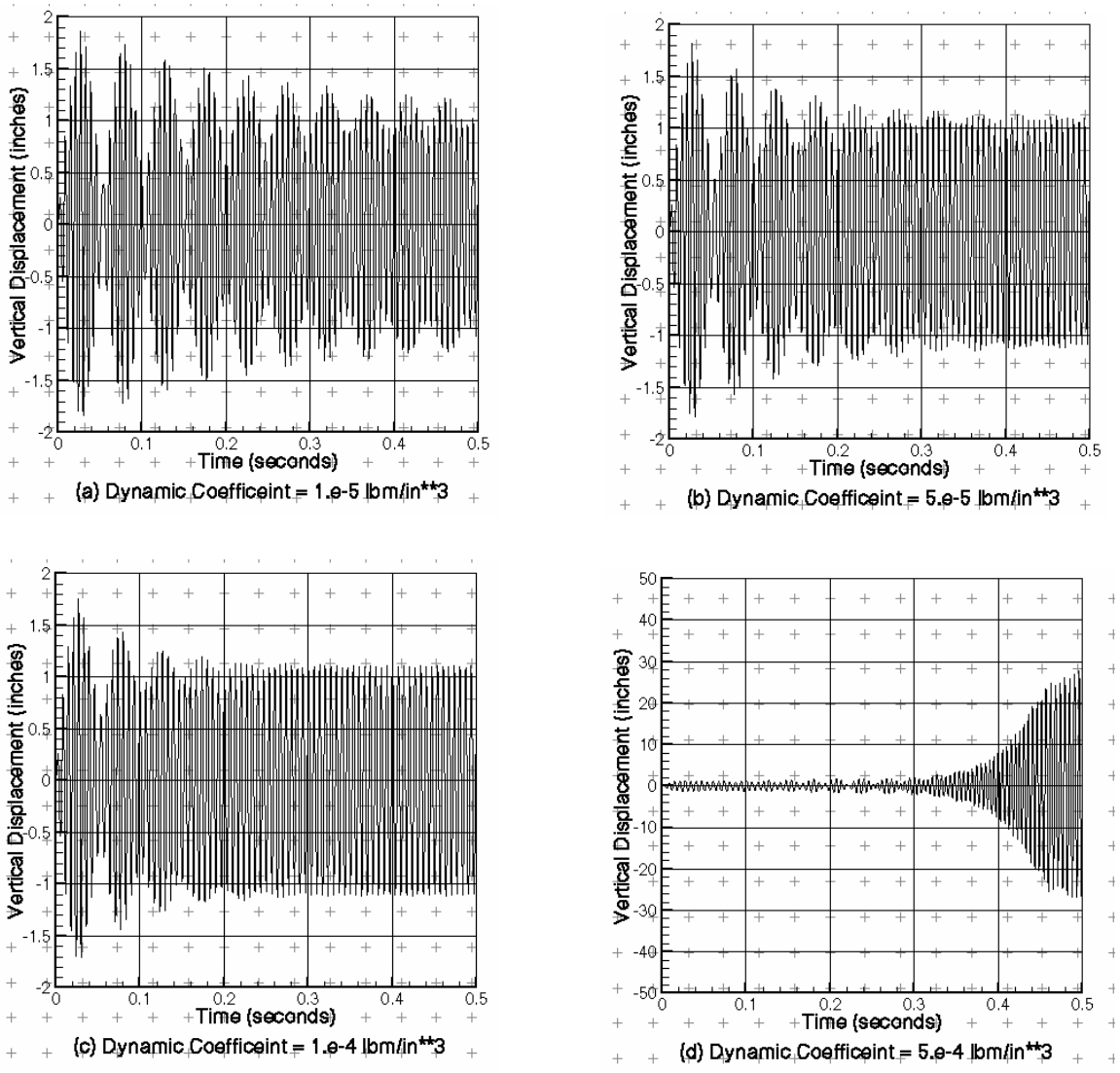

Figure 14: Effect of dynamic coefficient on transient response (3% structural damping, 30 degree blade angle of attack).

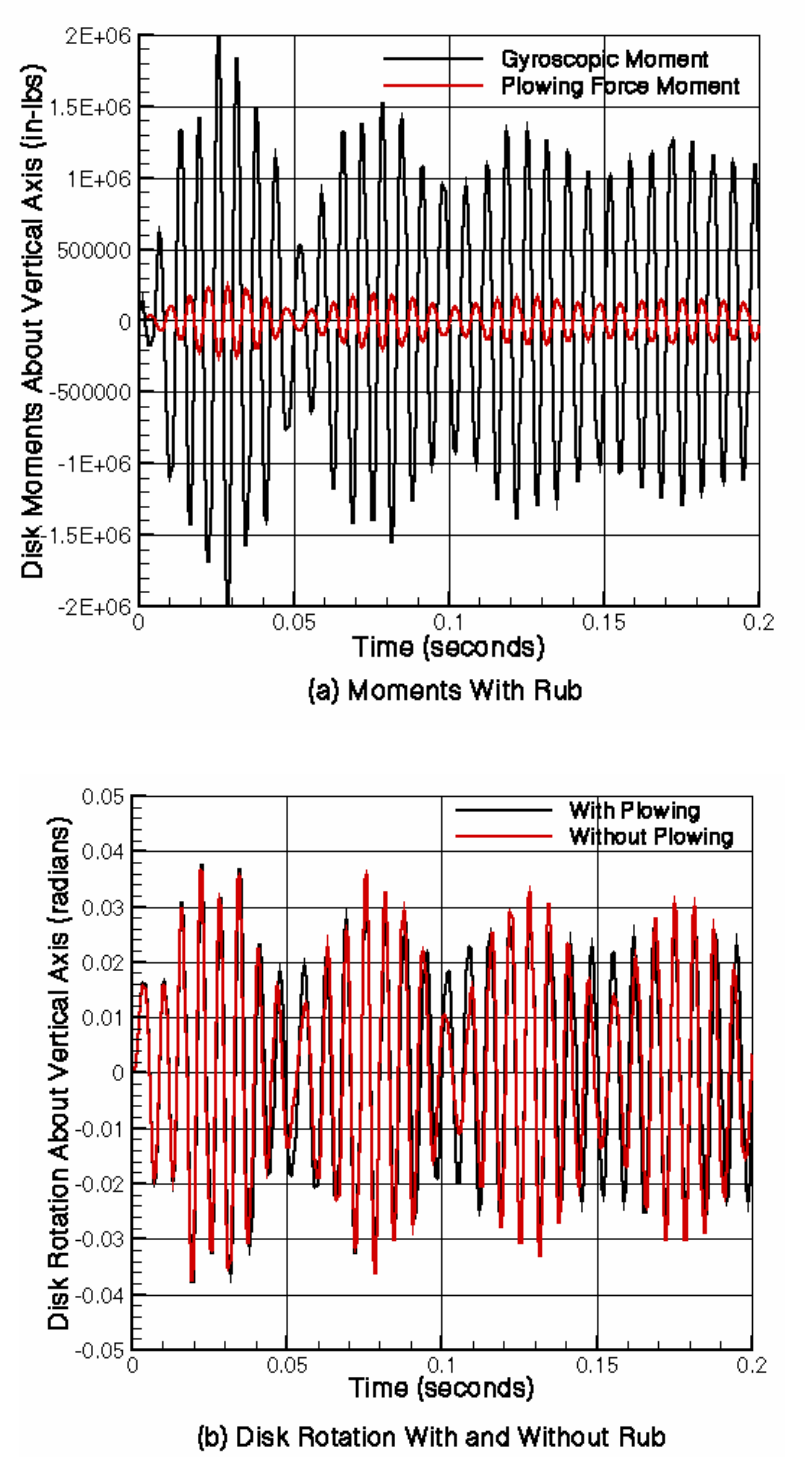

Figure 15: Effect of plowing force axial component on rotor response (3% structural damping, 30 degree blade angle of attack, dynamic coefficient = 1.e-4 lbm/in**3).

REPORT DOCUMENTATION PAGE

Form Approved
OMB No. 0704-0188

1. AGENCY USE ONLY (*Leave blank*)	2. REPORT DATE	3. REPORT TYPE AND DATES COVERED
	March 2003	Technical Memorandum

4. TITLE AND SUBTITLE

A Study of Fan Stage/Casing Interaction Models

5. FUNDING NUMBERS

WBS–22–728–30–07

6. AUTHOR(S)

Charles Lawrence, Kelly Carney, and Vicente Gallardo

7. PERFORMING ORGANIZATION NAME(S) AND ADDRESS(ES)

National Aeronautics and Space Administration
John H. Glenn Research Center at Lewis Field
Cleveland, Ohio 44135–3191

8. PERFORMING ORGANIZATION REPORT NUMBER

E–13836

9. SPONSORING/MONITORING AGENCY NAME(S) AND ADDRESS(ES)

National Aeronautics and Space Administration
Washington, DC 20546–0001

10. SPONSORING/MONITORING AGENCY REPORT NUMBER

NASA TM—2003-212215

11. SUPPLEMENTARY NOTES

Charles Lawrence and Kelly Carney, NASA Glenn Research Center; Vicente Gallardo, Ohio Aerospace Institute, Brook Park, Ohio 44142. Responsible person, Charles Lawrence, organization code 5930, 216–433–6048.

12a. DISTRIBUTION/AVAILABILITY STATEMENT

Unclassified - Unlimited
Subject Categories: 39 and 07 Distribution: Nonstandard

Available electronically at http://gltrs.grc.nasa.gov

This publication is available from the NASA Center for AeroSpace Information, 301–621–0390.

12b. DISTRIBUTION CODE

13. ABSTRACT ***(Maximum 200 words)***

The purpose of the present study is to investigate the performance of several existing and new, blade-case interactions modeling capabilities that are compatible with the large system simulations used to capture structural response during blade-out events. Three contact models are examined for simulating the interactions between a rotor bladed disk and a case: a radial and linear gap element and a new element based on a hydrodynamic formulation. The first two models are currently available in commercial finite element codes such as NASTRAN and have been showed to perform adequately for simulating rotor-case interactions. The hydrodynamic model, although not readily available in commercial codes, may prove to be better able to characterize rotor-case interactions.

14. SUBJECT TERMS	15. NUMBER OF PAGES
Turbomachinery; Structural dynamics	36
	16. PRICE CODE

17. SECURITY CLASSIFICATION OF REPORT	18. SECURITY CLASSIFICATION OF THIS PAGE	19. SECURITY CLASSIFICATION OF ABSTRACT	20. LIMITATION OF ABSTRACT
Unclassified	Unclassified	Unclassified	